First-principles calculation of resonant x-ray emission spectra applied to ZnO

A. R. H. Preston, A. DeMasi, L. F. J. Piper, K. E. Smith, W. R. L. Lambrecht, A. Boonchun, T. Cheiwchanchamnangij, J. Arnemann, M. van Schilfgaarde, and B. J. Ruck

Phys. Rev. B **83**, 205106 — Published 16 May 2011

DOI: 10.1103/PhysRevB.83.205106

First principles calculation of resonant x-ray emission spectra applied to ZnO

A. R. H. Preston,* A. DeMasi, L. F. J. Piper, and K. E. Smith
Department of Physics, Boston University, 590 Commonwealth Ave., Boston, MA 02215

W. R. L. Lambrecht, A. Boonchun, T. Cheiwchanchamnangij, and J. Arnemann
Department of Physics, Case Western Reserve University, Cleveland, OH 44106-7079

M. van Schilfgaarde
School of Materials, Arizona State University, Tempe, AZ 85284

B. J. Ruck
The MacDiarmid Institute, School of Chemical and Physical Sciences, Victoria University of Wellington, PO Box 600, Wellington 6140, New Zealand
(Dated: March 21, 2011)

A framework for calculating the k-conserving component of K-edge resonant x-ray emission spectroscopy measurements of anisotropic solids is presented. The crystalline band structure is calculated using a quasiparticle self-consistent *GW* implementation. Coherent spectra are calculated in the Kramers-Heisenberg formalism, and the effect of the experimental geometry in the dipole approximation is fully considered. Coherent spectra are calculated for ZnO and successfully compared to previously measured data.

PACS numbers: 71.55.Gs, 78.70.En, 78.70.Dm, 71.15.Mb
Keywords: RXES; ZnO; GW

I. INTRODUCTION

X-ray emission spectroscopy (XES) is a powerful tool for probing the bulk electronic structure of crystalline systems. The photon-in–photon-out nature and thus large penetration depth of the technique means the bulk band structure is probed,[1] and insulators can be investigated as well as metals. The general two-step x-ray emission process begins with x-ray stimulated excitation of a core hole, followed by the decay of a valence band state to fill the empty state. When the core electron is excited into bands close to (~ 10 eV) the conduction band minimum (CBM) this process becomes resonant and a coherent term is measured along with the XES. In this regime we are measuring resonant XES (RXES).

General overviews of RXES and the theory behind it can be found in Refs. 2 and 3. However, there are few reports in the literature where the coherent part of the RXES (CRXES) have actually been calculated with *ab initio* techniques, especially where the electronic structure requires an in depth treatment.[4–7]

In this paper we present the results of an implementation of the Kramers-Heisenberg equation on top of a quasisiparticle self-consistent (QS)-*GW* band structure calculation. We give full consideration to the effect of dipole selection rules on the incoming and outgoing photons in different polarization and experimental geometries, enabling us to calculate spectra that are directly comparable to experiment.

The theoretical results are compared to the measured wurtzite zinc oxide (ZnO) oxygen K-edge RXES. The literature yields a number of ZnO XES studies,[8,9] and the present work can be considered a continuation of the results we first reported in Ref. 10. We focus on wurtzite ZnO for two reasons: first, it has shown potential for use in optoelectronic applications,[11] consequently there is interest in accurately determining the details of its band structure; second, it has a remarkably dispersive and anisotropic conduction band, as can be seen in the band structure figures below. These features mean that for excitation energies close to the CBM, and for specific experimental geometries, small unique areas of the Brillioun zone can be probed with RXES, making the material an ideal test case.

II. EXPERIMENT

The experimental spectra reproduced in this paper were reported in Ref. 10, where the full experimental details can be found. Briefly, the sample was a 500 nm ZnO epilayer, grown on epi-ready (0001) sapphire by plasma-assisted MBE.[12] The high crystalline quality of the film was confirmed by a number of standard techniques.[13] The x-ray spectroscopy was performed on the undulator beamline X1B at the National Synchrotron Light Source at Brookhaven National Laboratory. X1B is equipped with a spherical grating monochromator and a Nordgren-type emission spectrometer. The X1 undulator produces light which is linearly polarized in the horizontal plane of the lab (see below). The energy resolution over the O K-edge was approximately 0.20 eV and 0.37 eV for the incident and emitted photons, respectively.

The CRXES was extracted from the RXES by using the standard technique of subtracting as large a fraction of the XES possible while subject to the physical con-

straint that the resulting spectra are never negative.[2]

The zero point of the calculated energy axis was placed at the VBM. The need for this empirical alignment arises from the inherent difficulty in calculating the core-level excitation of several 100 eV on an absolute scale with a precision of 0.1 eV or better. The experimental energy and theoretical energy scales were then aligned by a rigid shift to reach best agreement between the respective valence bands. For our comparisons we estimate that the experimental VBM is located at 527.2 eV.

III. THEORY

A. The Kramers-Heisenberg implementation

The coherent or (more precisely) wavevector conserving contribution to RXES is described according to the Kramers-Heisenberg theory.[2,3] For a one-electron band structure model of the solid, the RXES can be described by the following cross-section:

$$\left[\frac{d\sigma}{d\Omega d\omega_2}\right]_{\alpha,\beta} \propto \sum_{\mathbf{k}\in \mathrm{BZ}} \sum_{c,v} \left| \frac{\langle s|p_\alpha|c\mathbf{k}\rangle\langle v\mathbf{k}|p_\beta|s\rangle}{\epsilon_{c\mathbf{k}} - \epsilon_s - \omega_1 - i\Gamma_m/2} \right|^2 \times \delta(\omega_1 - \omega_2 - \epsilon_{c\mathbf{k}} + \epsilon_{v\mathbf{k}}). \quad (1)$$

Here, $\epsilon_{i\mathbf{k}}$, $i = (c, v)$ represent the single-particle band energies, while ω_1 corresponds to the incident (x-ray absorption) photon energy, which excites a dipole transition (p_α) from a core state (labeled s here with the oxygen K-edge in mind) with energy ϵ_s to a conduction band state $|c\mathbf{k}\rangle$, and ω_2 corresponds to the x-ray emission photon energy, resulting when a valence electron from a band state $|v\mathbf{k}\rangle$ (with the same wavevector) dipole-recombines with the core hole. The polarizations of the x-rays are labeled by α and β, respectively. The sum is over the full Brillouin zone (BZ) and we used units in which $\hbar = 1$. The above equation is obtained in the long-wave length approximation, neglecting the photon wave vectors as will be discussed at the end of this section.

The (full width at half max) lifetime broadening factor of the core hole is given by Γ_m where m refers to a specific intermediate state corresponding to the core hole and an electron excited to a conduction band $\epsilon_{c\mathbf{k}}$. The core hole lifetime of order fs[14] ($\Gamma_m \approx 0.1$ eV) ensures that for a given x-ray absorption energy only band states in a narrow energy range will contribute strongly when the energy denominator is resonant.

The energy conservation delta function indicates that the difference in energy between the absorbed and emitted photons must equal a vertical interband transition (constant wave vector). In other words, the x-ray absorption energy makes a horizontal slice (constant energy) through the band structure energies and we then obtain contributions from the vertical interband transitions for those $\mathbf{k}$-points and bands for which the matrix elements are non-zero by the selection rules. So, the required calculation is essentially like that of an interband optical dielectric function except that now the matrix elements involve the resonant factor which contains a product of two momentum matrix elements coupling both the conduction and valence band states to the same core state. Furthermore, we plot it not directly as function of the interband energy but as function of ω_2, the x-ray emission energy.

In practice, it is difficult to calculate the absolute energy of the core level with sufficient precision because of the so-called relaxation energy. This term refers to the fact that the orbitals adjust in the presence of the core hole. One could attempt this with so-called ΔSCF calculations, i.e. calculating the total energy difference between the system without and with a localized hole using an impurity type calculation. However, we can avoid this problem by allowing ourselves to use an empirical alignment of the calculated and experimental spectra as already mentioned above. In that case, all we need in the calculation is the spectrum relative to the highest XES energy, which corresponds to the VBM. Thus we write $\omega_1 = \epsilon_{\mathrm{VBM}} - \epsilon_s + \Delta\omega_1$, where ϵ_{VBM} is the energy of the valence band maximum (VBM). The x-ray emission energy is simimarly written as $\omega_2 = \epsilon_{\mathrm{VBM}} - \epsilon_s + \Delta\omega_2$. Note that in the RXES spectrum $\Delta\omega_2 < 0$ and is measured relative to the VBM. Returning to Eq. (1), the resonant factor can therefore be written as $(\epsilon_{c\mathbf{k}} - \epsilon_{\mathrm{VBM}} - \Delta\omega_1 - i\Gamma/2)^{-1}$, and the delta-function as $\delta[\Delta\omega_1 - \Delta\omega_2 - (\epsilon_{c\mathbf{k}} - \epsilon_{v\mathbf{k}})]$. In the results below, the XAS energy refers to $\Delta\omega_1$ and the XES energy refers to $\Delta\omega_2$.

The optical matrix elements between core states and band states are readily calculated in an all-electron method based on a muffin-tin type augmentation method such as the linearized augmented plane wave (LAPW) or linearized muffin-tin orbital (LMTO) method. We here use a full-potential FP-LMTO method.[16,17] The contribution from each eigenstate to partial waves in the muffin-tin sphere are readily obtained from the eigenvectors of the band structure problem and the augmentation properties of the basis functions to radial solutions inside each sphere. They contain so-called ϕ (the radial wavefunction at the linearization energy) and its energy derivative, $\dot{\phi}$ parts and in our particular implementation may also contain so-called local orbital contributions[18] for semi-core states. The integration over the Brillouin zone is similar to that used in the calculation of the optical joint density of states; in this case the integration is performed by a simple sampling method with the delta function broadened by a Gaussian of about 0.2 eV.

A key approximation in our current implementation of CRXES is that the two band states involved occur at the same $\mathbf{k}$-point. This assumes the wavevector of the x-ray is negligible compared to the size of the BZ. Strictly speaking there is a crystal momentum conservation delta function $\delta_{\mathbf{k}_1+\mathbf{q}_1-\mathbf{k}_2-\mathbf{q}_2}$, where $\mathbf{k}_1$ is the $\mathbf{k}$-point of the conduction band state involved in the x-ray absorption, $\mathbf{q}_1$ is the wavevector of the absorbed x-ray, $\mathbf{k}_2$ is the $\mathbf{k}$-point of the valence band in the x-ray emission part of the process, and $\mathbf{q}_2$ is the wavevector of the emitted x-

ray. So, it is the difference between emitted and absorbed x-ray wavectors we assume to be negligible.[15] The overall crystal momentum conservation used here assumes that the intermediate states with the core hole do not break the crystal periodicity.

B. Band structure calculation

The above methodology can be applied with different underlying approximations to the potential for the band structure problem, the most commonly used of which is the local density approximation for exchange and correlation.[20,21] Here we use the quasiparticle self-consistent *GW* approach.[22] In this approach, a non-local exchange-correlation potential

$$V_{xc}^{QSGW} = \frac{1}{2}\sum_{nm} |\psi_m\rangle \Re\{\Sigma_{mn}(\epsilon_m) + \Sigma_{mn}(\epsilon_n)\}\langle\psi_n|, \quad (2)$$

is used, constructed from the *GW* self-energy operator, whose matrix element $\Sigma_{mn}(\epsilon)$ is written in the basis of the eigenstates of the independent particle Hamiltonian with this exchange correlation potential. The latter is chosen such that the Kohn-Sham eigenvalues converge to the quasiparticle excitation energies in the *GW* approximation. In the *GW* approximation, the self-energy is schematically written as $iG^0 \times W$ with G^0 the one-electron Green's function corresponding to the Kohn-Sham Hamiltonian and W the screened Coulomb interaction. The latter is given by $W = \varepsilon^{-1}v = (1 - \Pi v)^{-1}v$ with v the bare Coulomb interaction and Π the independent particle polarizability $\Pi = -iG^0 \times G^0$, ε being the dielectric function. Starting from the LDA Hamiltonian, one constructs a *GW* self-energy, Σ^0, from which a new V_{xc} is obtained through Eq. (2), from which a new *GW* self-energy is obtained, and so on, until self-consistency is reached.

Strictly speaking the matrix elements in the Kramers-Heisenberg formalism should be velocity matrix elements and involve the commutator $[\mathbf{r}, H]$ which is not purely the momentum operator if a non-local potential is included.[23] We ignore this complication for now, which corresponds to making the usual long-wavelength approximation and is consistent with our assumption of neglecting the momentum of the photon. The (QS)-*GW* is implemented in terms of a mixed basis set for expanding any two-particle operator (v, W, Π, Σ). This mixed basis includes plane waves projected on the interstitial space and product basis functions of LMTOs in the spheres.[24] The (QS)-*GW* approach in this all-electron implementation has been shown to give excellent and very systematic results for a wide variety of systems. It slightly overestimates most semiconductor band gaps, which can be traced to the use of the random phase approximation (RPA) of the polarizability. One finds in practice that a mixture of $0.8V_{xc}^{QSGW} + 0.2V_{xc}^{LDA}$ gives almost exact agreement with the experimental band gaps. We obtain a band gap of 3.48 eV (*c.f.* the experimental value of 3.4 eV[25]) for ZnO in this way, not including spin-orbit coupling, nor zero-point motion corrections or exciton binding energy corrections.

The reader might wonder if expensive GW calculations are necessary for describing RXES. As mentioned, the theory involves interband transitions, so some correction to the gap is necessary. However, to see the changes from k-point to k-point what matters most is the dispersion of the bands in the valence and conduction bands separately. So, one could probably obtain similar results by just adding a constant gap shift to the LDA calculations. Nonetheless, the QS-*GW* approximation is also expected to improve band widths and dispersions compared to LDA.[24] Not all conduction band shift by the same amount between GW and LDA. Details about the present GW calculations for ZnO, including the position of the Zn3*d* bands can be found in Kotani et al.[22].

The (QS)-*GW* exchange-correlation potential can be re-expanded from the eigenstates on a relatively coarse **k**-mesh to the LMTO basis set in real space via an inverse Bloch transformation and then evaluated for a fine **k**-point mesh. This capability is important here because we need a fine **k**-point mesh to properly calculate the joint density of states like interband transitions spectral function in CRXES. If the **k**-point mesh is too coarse, the resonant factor is not effective in picking out the resonant contributions. Symmetrization of the matrix elements $|\langle s|p_\alpha|c\mathbf{k}\rangle|^2$ and $|\langle s|p_\alpha|v\mathbf{k}\rangle|^2$ is performed over all point group elements, so the integration can still be done over the irreducible part of the Brillouin zone. We calculate the full 3×3 matrix of cross-sections for different incoming and outgoing x-ray polarizations.

C. Angular dependence and experimental geometry

From Eq. (1) we can see that dipole selection rules may lead to an angular dependence of the RXES cross-section, which from here on we will write as $M_{\alpha\beta}$. More specifically, if we restrict ourselves to K-edge spectra, the s-like core hole implies that only matrix-elements to p-orbital contributions to the conduction band and valence band states enter the two dipole moment matrix elements. The indices α, β in Eq. (1) are the Cartesian components of the momentum operators of the XAS and XES parts of the process respectively, which are determined by the polarizations $\mathbf{e}_i$, $\mathbf{e}_o$ of the incoming and outgoing beam. Depending on the crystal symmetry, several independent cross-sections exist. Let us call the matrix elements of the XAS and XES momentum operators $\mathbf{p}^{XAS}$ and $\mathbf{p}^{XES}$ respectively, which are both vectors. The angular dependence of the cross-sections is then determined by $|\mathbf{e}_i \cdot \mathbf{p}^{XAS}|^2 |\mathbf{p}^{XES} \cdot \mathbf{e}_o|^2$. For example, for a hexagonal crystal such as wurtzite ZnO, there are 4 independent components, M_{11}, M_{33}, M_{13} and M_{31}, where 3 refers to the c-axis of the crystal and 1 to a direction perpendicular to the c-axis. Note however that the matrix $\mathbf{M}$ is

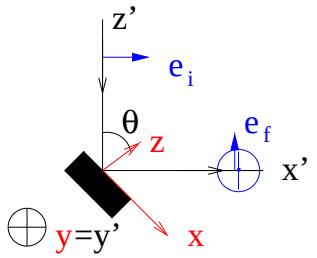

FIG. 1. (Color on-line) The X1B experimental geometry. The lab coordinates x', y', z' (black) and the sample coordinates x, y, z (red) are shown. Photons (black arrows) are incident along z' and emitted photons are collected along x'. The angle between the sample normal and the incident beam, θ, is freely changed during the experiment.

not symmetric because the first index refers to XAS and the second to the XES parts of the process, which are different. In general, we may have up to 9 independent components.

While from a theory point of view, it is natural to describe the polarization directions relative to the crystalline symmetry axes, from an experimental point of view, the polarization directions are determined by the experimental geometry. Thus, different fractions of the independent components of the cross-section matrix $\mathbf{M}$ enter the experimentally measured cross-section. Essentially, we just need to know the projections of the incoming and outgoing polarization unitvectors on the relevant crystal axes. If $\mathbf{e}^{XAS}$ is a unit vector along the XAS momentum matrix element and $\mathbf{e}^{XES}$ a unit vector along the XES momentum matrix element, then we generally have that

$$M_{io} = |\mathbf{e}_i \cdot \mathbf{e}_\alpha^{XAS}|^2 M_{\alpha,\beta} |\mathbf{e}_o \cdot \mathbf{e}_\beta^{XES}|^2, \tag{3}$$

where summation over repeated indices is understood.

The experimental conditions can be changed in a number of ways: the polarization of the photons can be altered; the position of the spectrometer can be changed; the sample can be rotated; and different cleavage planes of the same sample can be chosen. It is convenient here to consider three sets of coordinates, the lab frame coordinates (x', y', z'), the coordinates fixed to the sample with a specific cleavage plane (x, y, z), and the coordinates corresponding to the natural symmetry axis of the crystal $(1, 2, 3)$.

As an example, we consider the setup at beamline X1B, which is sketched in Fig. 1. The undulator at X1B provides light (incident along z') polarized linearly along x'. The emission spectrometer is mounted perpendicular to the incoming photon in the x' direction, but does not itself resolve polarization. Finally, the sample is mounted on a manipulator that allows us to rotate the sample about y'. On the other hand, the z axis is defined to be normal to the cleavage plane of the sample, the x axis is the intersection of the cleavage plane with the incident plane, *i.e.* the plane spanned by the normal to the sample, and the incoming as well as the outgoing beam, and $y = y'$. In other words, we here always use so-called p-polarized incoming x-rays. The orientation of the sample is determined by θ, the angle between the incoming beam and the normal to the sample, *i.e.* between z' and z. We thus have

$$\mathbf{e}_i \cdot \mathbf{e}^{XAS} = e_x^{XAS} \cos\theta + e_z^{XAS} \sin\theta, \tag{4}$$

$$\mathbf{e}_o \cdot \mathbf{e}^{XES} = e_x^{XES} \sin\theta\cos\phi + e_y^{XES} \sin\phi + e_z^{XES} \cos\theta\cos\phi, \tag{5}$$

and we need to average over all possible emitted photon polarization angles in the $z'y'$ plane, ϕ. Since each polarization factor enters modulo squared for input and output, integrating over the $\cos^2\phi$ and $\sin^2\phi$ factors simply gives a constant factor, $1/2$, and we obtain for the total CRXES cross-section

$$M = \frac{1}{2}[\sin^2\theta\cos^2\theta(M_{xx} + M_{zz}) + \sin^4\theta M_{zx} + \cos^4\theta M_{xz} + \sin^2\theta M_{zy} + \cos^2\theta M_{xy}]. \tag{6}$$

However, here x, y, z are not yet referred to the crystalline symmetry axes but merely to the sample position in the lab. For a general cleavage plane with Miller indices (hkl), the surface normal is $G_{hkl}/|G_{hkl}|$, which can be expressed in terms of the crystal symmetry axes, $\hat{1}, \hat{2}, \hat{3}$. Let $\hat{x} = \sum_i a_i \hat{x}_i$, $\hat{y} = \sum_i b_i \hat{x}_i$, and $\hat{z} = \sum_i c_i \hat{x}_i$. We can then construct a matrix,

$$\mathbf{R} = \begin{pmatrix} |a_1|^2 & |a_2|^2 & |a_3|^2 \\ |b_1|^2 & |b_2|^2 & |b_3|^2 \\ |c_1|^2 & |c_2|^2 & |c_3|^2 \end{pmatrix}, \tag{7}$$

which allows us to transform from xyz sample coordinates to the crystal axes coordinates,

$$M_{ij} = R_{i\alpha} M_{\alpha\beta} R^T_{\beta j}. \tag{8}$$

Combining these steps we write that the measured cross section is given by

$$M \propto \left(\cos^2\theta, 0, \sin^2\theta\right) \mathbf{RMR}^T \begin{pmatrix} \sin^2\theta \\ 1 \\ \cos^2\theta \end{pmatrix}. \tag{9}$$

In the specific case of a hexagonal crystal cleaved along the c-plane the $\mathbf{R}$ matrix is just a unit matrix thus, taking into account the symmetries $M_{11} = M_{22} = M_{12} = M_{21}$, we immediately obtain

$$M \propto M_{11}\cos^2\theta(\sin^2\theta + 1) + M_{13}\cos^4\theta + M_{31}\sin^2\theta(\sin^2\theta + 1) + M_{33}\sin^2\theta\cos^2\theta. \tag{10}$$

For the M-plane $(1\bar{1}00)$ cleave, with $[000\bar{1}]$ oriented along x, we obtain

$$M \propto M_{11}(1 + \cos^2\theta)\sin^2\theta + M_{13}\sin^4\theta + M_{31}(1 + \cos^2\theta)\cos^2\theta + M_{33}\sin^2\theta\cos^2\theta,$$

while for the M-plane with $[11\bar{2}0]$ oriented along x, we obtain

$$M \propto M_{11} + M_{13}. \tag{11}$$

The angular dependence of the components is quite striking. As θ is increased from zero, at normal incidence, to grazing incidence the components that contribute to the measured RXES vary significantly. For the c-plane, there are strong initial contributions from both M_{11} and M_{13}. Note that one cannot simply separate $p_\perp = \{p_x, p_y\}$ (M_{11}) from p_z (M_{13}) emmitted components for near normal incidence. This is because the XES is not polarization filtered. In the mid-range all components contribute, while at large angles the contribution from M_{31} dominates. For the M-plane, the angular behaviour depends also on the in-plane sample orientation. When the c-axis $[000\bar{1}]$ is oriented toward the emission spectrometer the situation is obviously a continuation of the c-plane geometry (*i.e.* $\theta' = \theta + \pi/2$). However, when $[11\bar{2}0]$ is oriented along x there is no angular dependence at all.

The above derivations allow us to simulate any measured spectra directly in terms of the calculated cross-sections. On the other hand, it is clear that if we consider n independent choices of measurement angle and cleavage plane, we obtain n equations from which we can extract the $n(\leq 9)$ unique cross-sections experimentally and from there can predict those for other angles or cleavage planes. This is of use in cases where the band structure cannot (yet) be calculated to high accuracy *i.e.* strongly correlated systems.

IV. RESULTS

A. Band structure

The band structure, weighted by $p_\perp$ and p_z, is shown in Fig. 2. The bands and weightings agree well with previously published results.[10] In particular, the lowest conduction band has low effective mass and strong $p_\perp$ character along M-Γ-K (the $p_\perp$ orbitals lie in the M-Γ-K plane), p_z character along Γ-A (p_z orbitals point in the Γ-A direction) and mixed character along trajectories toward L and H. The top 6 eV of the valence band is comprised of O p-like states. Along Γ-A, the top two weakly dispersing bands have $p_\perp$ character, while the third and fourth bands are p_z-like and disperse to a lower energy near A. The flat bands at about -7 eV are Zn $3d$ derived, but the weightings show that there is significant p-like character to them.

B. CRXES measurement and calculation

Fig. 3 shows the CRXES for c-plane wurtzite ZnO at near normal (NN, $\theta = 20°$) and near grazing (NG $\theta = 70°$) incidence. Both measured and calculated spectra are shown; the calculated cross-sections have been properly weighted for experimental geometry. The calculations show more detailed peak structure and stronger anisotropy and dispersion effects than the experiments. At least in part, this is related to the difficulties in extracting the coherent fraction CRXES from the total XES which contains a significant incoherent fraction (see above). Further, the measured RXES are broadened by the emission spectrometer resolution of 0.37 eV.[19]

For the most part, however, good agreement is obtained between theory and experiment. Indeed qualitative trends in the spectra can be directly related to the band structure dispersion as discussed in Ref. 10. For NN measurements, the incident photons will couple predominantly to the $p_\perp$ orbitals and thus any coherent emission must come from the M-Γ-K part of the Brillouin zone, at least for low photon energy. For NG incidence, the incident photons will couple to the p_z orbitals and thus the Γ-A part of the Brillouin zone. At higher photon energies the conduction bands become less dispersive and larger parts of the Brillouin zone start to contribute to the CRXES. Above about 6 eV both NN and NG spectra will see contributions from L-A-H, and at larger energies still, above about 10 eV, it is very difficult, without *ab initio* techniques, to isolate specific contributions to the measured spectra.

For NG incidence, only the $p_\perp$ dominated bands will contribute significantly to the emission because both the s-polarized and p-polarized contributions are perpendicular to the c-axis of the crystal. Thus, to a first approximation, the p_z conduction bands and $p_\perp$ valence bands from Fig. 2 can be used to consider NG CRXES (this is the same as saying that M_{31} dominates). However for NN incidence, both the $p_\perp$ and p_z weighted valence bands will contribute to the emission because we did not resolve the polarization of the emitted x-rays (both M_{11} and M_{13} contribute).

We now describe the trends in the figure, starting with the NG spectra. The experimental spectra consist of a strong peak between 0 and -3 eV which at high incident energies develops a high binding energy tail down to about -5 eV. These are the so-called O $2p$ bands. The weak peak near about -8 eV is due to emission from O $2p$ states hybridized with the Zn $3d$ semi-core states.

According to the band plots and our analysis of the angular effects, the upper peak should initially derive from the upper two valence bands along Γ-A, which approach each other as we move toward A. However by the third and fourth measured spectra the incident energy is already large enough to be moving upward along A-H and A-L in the conduction bands. Along these directions, the upper valence bands of $p_\perp$ character disperse significantly downward and this explains the basic downward dispersion of the upper peak in the CRXES. We start picking up the bands near -5 eV by the time we are at incident energies of 7.9 eV (4th measured spectrum from the bottom). This is because near L and H the valence bands near -5 eV have a significant $p_\perp$ character. Near 10–11 eV incident energy, the region near Γ starts con-

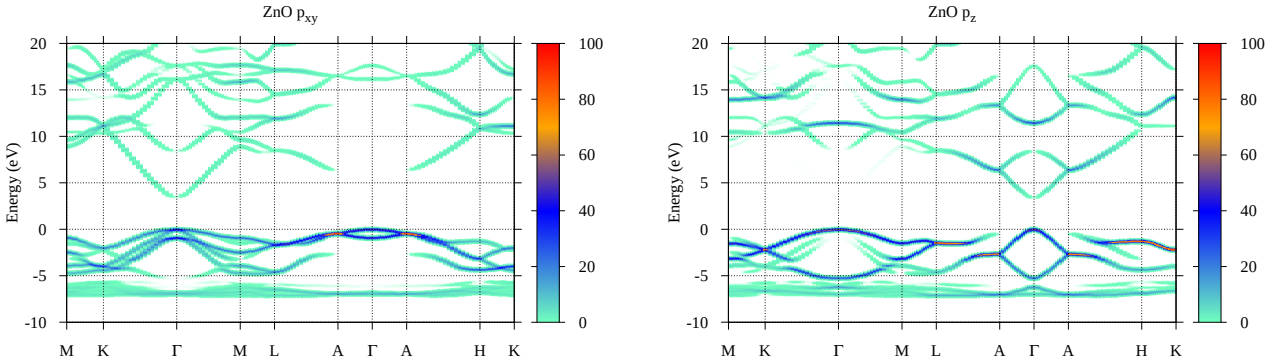

FIG. 2. (Color on-line) Intensity map of the calculated band structure. The intensity of each band is proportional to the p_{xy} (left) and p_z (right) character of the band at that point in the Brillouin zone.

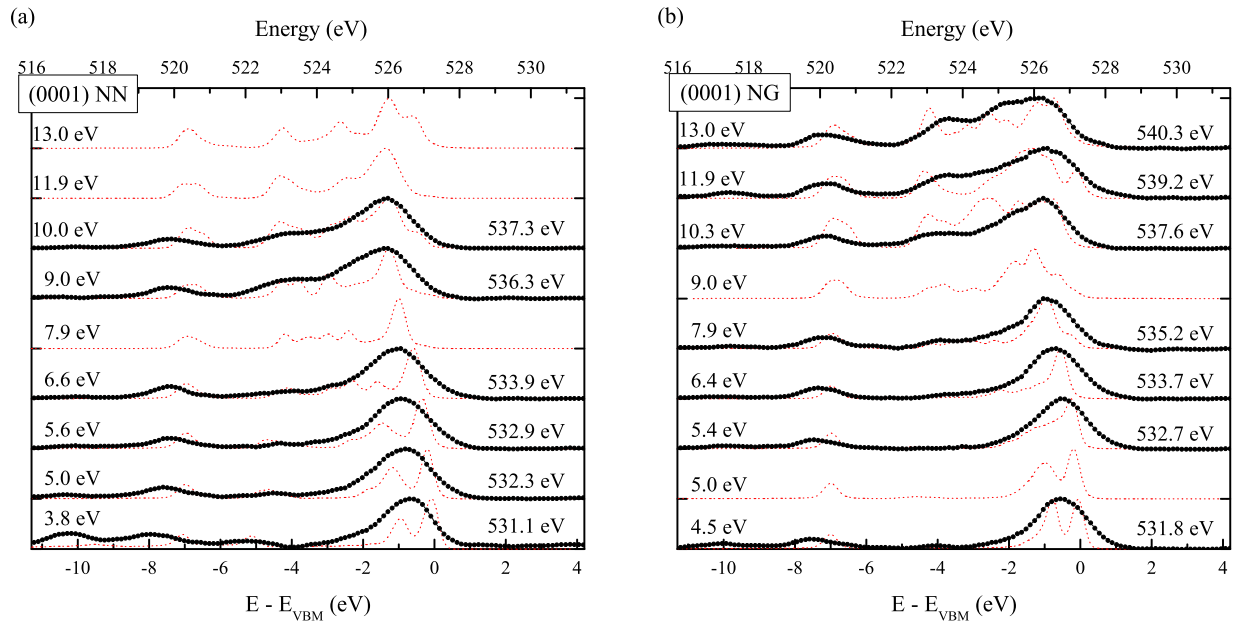

FIG. 3. (Color on-line) Calculated (dashed red lines) and measured (solid black circles) ZnO (0001) CRXES at (a) near normal (20°), and (b) near grazing (70°) incidence. Each spectrum is labelled with its excitation energy; photon energy on the right, and energy relative to the VBM on the left.

tributing because the third conduction band here has p_z character. This leads to a valence band contribution at low binding energy which broadens the upper peak and shifts it to lower binding energy. Near 13 eV incident energy conduction bands near M acquire a p_z contribution and the corresponding valence bands contribute, leading overall to broader and more complex upper peak. The d-like bands also show a broader and stronger contribution at this XAS energy.

As mentioned above, the situation is a little more complicated for NN spectra as we must consider both the $p_\perp$ and p_z valence bands. The p_z contribution means we can right away see a contribution from the lower valence bands near -5 eV which disperse upward with increasing energy, while the main peak from the VBM disperses downward. At an incident energy of 9.0 eV the contribution is from M and largely from K, where the highest valence band lies at about -3 eV. This explains the strong downward shift in the main peak. At 10 eV and above the bands are less dispersive and more regions of the BZ contribute to the CRXES leading to more features in the spectra, but there is clearly no contribution from Γ, as was seen for the NG case.

While the spectra for the two geometries were not

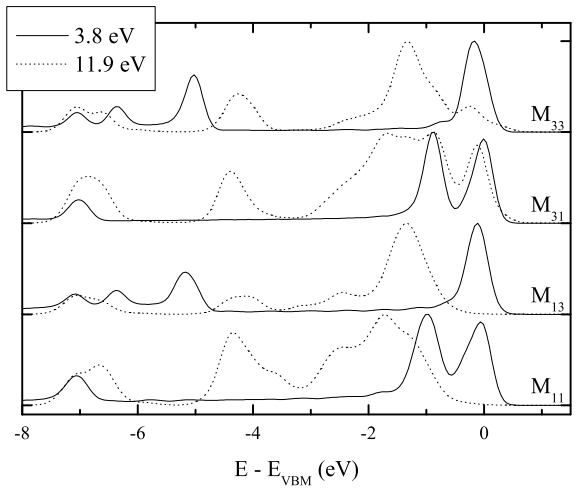

FIG. 4. The four unique CRXES cross-sections, calculated for excitation energies of 3.8 (solid lines) and 11.9 eV (dashed lines).

taken at exactly the same excitation energies[26], it is clear (from the calculation) that the XES shows rather smooth and continuous changes with XAS excitation energy. The good agreement between theory and experiment is further evidence that the changes observed are truly due to the anisotropy and not to the small changes in excitation energy between the two different geometries.

C. Extracting band structure information from CRXES

One somewhat overlooked feature of CRXES is the ability to resolve conduction bands in both energy and **k**-space. The canonical example is to determine nature of the band-gap of a semiconductor via dispersion close to the CBM. If ZnO is a direct-gap semiconductor the CRXES will disperse to higher binding energy with increasing photon energy, while the opposite will happen for an indirect-gap semiconductor.[2] The former is clearly seen in the four lowest excitation energies of both the NN and NG CRXES in Fig 3.

It is also possible to extract information about higher conduction bands. Note that for an incident photon energy of 539.2 eV (11.9 eV above the VBM) a spectral shift to lower binding energy is clearly resolved in the NG CRXES of Fig. 3. This must be due to a contribution from the VBM, given the similarity to the lowest excitation energy spectrum. The VBM is at Γ and for NG CRXES the incoming photons couple largely to bands of p_z character, therefore we can deduce that there is a flat conduction band 11.9 eV above the VBM located at Γ with p_z character.

We have made these deductions independently of the calculated band structure or complementary experimental techniques, like x-ray absorption spectroscopy (XAS). This method for locating conduction bands has advantages over XAS. In coherent emission, the core hole is assumed not to alter the valence and conduction band states at the time scale of the combined processes of absorption and emission (see Ref. 28). If this were not the case, the **k**-conservation rule would be broken. In contrast, in XAS the usual final state rule implies that the conduction band states are relaxed in the presence of the core hole localized at some particular location in the crystal, and hence are more representative of the local density of states around a $Z + 1$ impurity than of the unperturbed material. So it is much more accurate to locate the unperturbed conduction bands relative to the valence bands in CRXES.

Figure 4 shows the four components of the calculated CRXES for excitation energies of 3.8 and 11.9 eV. For both excitation energies there is a strong peak due to the VBM at 0 eV. This peak is seen in all four components of the 3.8 eV spectrum, but only in the M_{31} component of the 11.9 eV spectrum. This is fully consistent with the conclusions from the experiment above.

We turn now to the Zn 3*d*-derived part of the spectra, located below −6 eV in Fig. 4. At 3.8 eV excitation energy the M_{13} and M_{33} spectra have a double-peak structure. This can be traced to the crystal field splitting of the 3*d* bands at Γ. Similar dispersion has been observed in ARPES measurements of the ZnO valence band.[29]. We note here that the final states of CRXES and ARPES measurements are quite different, and that CRXES measures what is effectively emission from O 2*p* states hybridized with Zn 3*d* states, as opposed to directly interrogating the 3*d* electrons, providing a complementary method for investigating these bands.

V. CONCLUSION

We presented a general framework for calculating the K-edge CRXES of crystalline systems, including matrix elements connecting the valence and conduction band states to the core wave function, and full consideration of experimental geometry and polarization effects. Explicit calculations of the CRXES of wurtzite ZnO were compared to measurements. Good agreement was obtained with experimental data. The analysis of the angular effects in our RXES set up was revisited and shows that because at present the emitted x-ray is not polarization filtered the possibility to filter valence bands according to the orbital weights is somewhat restricted. However, the XAS polarization filtering and use of NN or NG incidence still allows to focus on different portions of the BZ. The entirely parameter free (QS)-*GW* results overall provide an excellent account of the spectral features.

ACKNOWLEDGMENTS

Funding for the BU group is provided by the DOE (DE-FG02-98ER45680) and donors of the American Chemical Society Petroleum Research Fund The NSLS is supported by the DOE (DE-AC02-98CH10886). The work at CWRU and BU is supported by the Materials World Network NSF grant No. DMR-0710485. BR was supported by New Economy Research Fun Grant No. VICX0808). MvS was supported by NSF Grant No. QMHP-0802216.

* andrew.preston@gmail.com; http://preston.co.nz

[1] S. Eisebitt, T. Böske, J.-E. Rubensson, and W. Eberhardt, Phys. Rev. B, **47**, 14103 (1993).

[2] S. Eisebitt and W. Eberhardt, J. Elec. Spec. and Rel. Phenom., **110**, 335 (2000).

[3] A. Kotani and S. Shin, Rev. Mod. Phys., **73**, 203 (2001).

[4] J. A. Carlisle, E. L. Shirley, L. J. Terminello, J. J. Jia, T. A. Callcott, D. L. Ederer, R. C. C. Perera, and F. J. Himpsel, Phys. Rev. B, **59**, 7433 (1999).

[5] D. Eich, O. Fuchs, U. Groh, L. Weinhardt, R. Fink, E. Umbach, C. Heske, A. Fleszar, W. Hanke, E. K. U. Gross, C. Bostedt, T. v. Buuren, N. Franco, L. J. Terminello, M. Keim, G. Reuscher, H. Lugauer, and A. Waag, Phys. Rev. B, **73**, 115212 (2006).

[6] J. A. Carlisle, E. L. Shirley, E. A. Hudson, L. J. Terminello, T. A. Callcott, J. J. Jia, D. L. Ederer, R. C. C. Perera, and F. J. Himpsel, Phys. Rev. Lett., **74**, 1234 (1995).

[7] L. Weinhardt, O. Fuchs, A. Fleszar, M. Bär, M. Blum, M. Weigand, J. D. Denlinger, W. Yang, W. Hanke, E. Umbach, and C. Heske, Phys. Rev. B, **79**, 165305 (2009).

[8] C. McGuinness, C. B. Stagarescu, P. J. Ryan, J. E. Downes, D. Fu, K. E. Smith, and R. G. Egdell, Phys. Rev. B, **68**, 165104 (2003).

[9] C. L. Dong, C. Persson, L. Vayssieres, A. Augustsson, T. Schmitt, M. Mattesini, R. Ahuja, C. L. Chang, and J.-H. Guo, Phys. Rev. B, **70**, 195325 (2004).

[10] A. R. H. Preston, B. J. Ruck, L. F. J. Piper, A. DeMasi, K. E. Smith, A. Schleife, F. Fuchs, F. Bechstedt, J. Chai, and S. M. Durbin, Phys. Rev. B, **78**, 155114 (2008).

[11] A. P. Ramirez, Science, **315**, 1377 (2007).

[12] W. C. T. Lee, M. Henseler, P. Miller, C. H. Swartz, T. H. Myers, R. J. Reeves, and S. M. Durbin, J. of Elec. Mat, **35**, 1316 (2006).

[13] J. Kennedy, A. Markwitz, H. J. Trodahl, B. J. Ruck, S. M. Durbin, and W. Gao, J. of Elec. Mat, **36**, 472 (2007).

[14] J. Stöhr, *NEXAFS Spectroscopy*, 2nd ed., Springer Series in Surface Sciences (Springer, 2003).

[15] The self-energy shift is often referred to as the relaxation energy in the context of core-level spectroscopy.

[16] M. Methfessel, M. van Schilfgaarde, and R. A. Casali, in *Electronic Structure and Physical Properties of Solids. The Use of the LMTO Method*, Lecture Notes in Physics, Berlin Springer Verlag, Vol. 535, edited by H. Dreyssé (2000) p. 114.

[17] T. Kotani and M. van Schilfgaarde, Phys. Rev. B, **81**, 125117 (2010).

[18] D. Singh, Phys. Rev. B, **43**, 6388 (1991).

[19] We note that at the O K-edge ($\sim$ 530 eV), the photon momentum is $\mathbf{q} = E/(\hbar c) \approx 0.27$ Å^{-1}, or roughly 0.14 of the Brillouin zone. The outgoing vector $\mathbf{q}_2$ is perpendicular to the incoming wavevector and hence $\mathbf{k}_2 - \mathbf{k}_1 = \mathbf{q}_1 - \mathbf{q}_2 \approx 0.2$ of the BZ.

[20] P. Hohenberg and W. Kohn, Phys. Rev., **136**, B864 (1964).

[21] W. Kohn and L. J. Sham, Phys. Rev., **140**, A1133 (1965).

[22] T. Kotani, M. van Schilfgaarde, and S. V. Faleev, Phys.Rev. B, **76**, 165106 (2007).

[23] S. H. Rhim, M. Kim, A. J. Freeman, and R. Asahi, Phys. Rev. B, **71**, 045202 (2005).

[24] M. van Schilfgaarde, T. Kotani, and S. V. Faleev, Phys.Rev. B, **74**, 245125 (2006).

[25] U. Özgür, Y. I. Alivov, C. Liu, A. Teke, M. A. Reshchikov, S. Doğan, V. Avrutin, S.-J. Cho, and H. Morkoç, J. Appl. Phys., **98**, 041301 (2005).

[26] The incident energy broadening is incorporated directly into the calculation.

[27] The latter were chosen in the experiment to coincide with interesting features in the XAS and predate the present theoretical analysis – see Ref 10.

[28] Y. Ma, Phys. Rev. B, **49**, 5799 (1994).

[29] L. F. J. Piper, A. R. H. Preston, A. Fedorov, S. W. Cho, A. DeMasi, and K. E. Smith, Phys. Rev. B, **81**, 233305 (2010).